PNAS RESEARCH ARTICLE | CELL BIOLOGY OPEN ACCESS

Molecular convergence by differential domain acquisition is a hallmark of chromosomal passenger complex evolution

Shinichiro Komaki[a,1], Eelco C. Tromer[b], Geert De Jaeger[c,d], Nancy De Winne[c,d], Maren Heese[e], and Arp Schnittger[e,1]

Edited by Detlef Weigel, Max-Planck-Institut für Biologie Tübingen, Tübingen, Germany; received January 12, 2022; accepted September 7, 2022

The chromosomal passenger complex (CPC) is a heterotetrameric regulator of eukaryotic cell division, consisting of an Aurora-type kinase and a scaffold built of INCENP, Borealin, and Survivin. While most CPC components are conserved across eukaryotes, orthologs of the chromatin reader Survivin have previously only been found in animals and fungi, raising the question of how its essential role is carried out in other eukaryotes. By characterizing proteins that bind to the *Arabidopsis* Borealin ortholog, we identified BOREALIN RELATED INTERACTOR 1 and 2 (BORI1 and BORI2) as redundant Survivin-like proteins in the context of the CPC in plants. Loss of BORI function is lethal and a reduced expression of *BORI*s causes severe developmental defects. Similar to Survivin, we find that the BORIs bind to phosphorylated histone H3, relevant for correct CPC association with chromatin. However, this interaction is not mediated by a BIR domain as in previously recognized Survivin orthologs but by an FHA domain, a widely conserved phosphate-binding module. We find that the unifying criterion of Survivin-type proteins is a helix that facilitates complex formation with the other two scaffold components and that the addition of a phosphate-binding domain, necessary for concentration at the inner centromere, evolved in parallel in different eukaryotic groups. Using sensitive similarity searches, we find conservation of this helical domain between animals and plants and identify the missing CPC component in most eukaryotic supergroups. Interestingly, we also detect Survivin orthologs without a defined phosphate-binding domain, likely reflecting the situation in the last eukaryotic common ancestor.

cell division | microtuble cytoskeleton | evolution

Significance

The chromosomal passenger complex (CPC) is a key regulator of the microtubule cytoskeleton, which is crucial for cell division. However, in many species, including plants, one central component of the CPC, called Survivin, which is important for the subcellular localization of the CPC, has not been detected so far. Here we present the identification of Survivin-type genes in plants and subsequently in most eukaryotes. We reveal a large variation in the structural organization of this component, yet with functional conservation, suggesting molecular convergent evolution and pinpointing to its ancient arrangement in the last common ancestor of all eukaryotes.

Proper chromosome segregation and cytokinesis are essential for every organism to accurately transmit its genomic information to its progeny. For both processes, a precise regulation of the microtubule cytoskeleton is of key importance in plants and other eukaryotes (1). First, the microtubule fibers of the spindle have to be attached to chromosomes so that they will be equally distributed during cell division. The attachment is accomplished and monitored by a conserved large multiprotein structure called the kinetochore, which assembles at the centromeres of chromosomes (2, 3). Second, microtubules need to be precisely arranged to accomplish cytokinesis following chromosome segregation. In animals, microtubules mark the future site of division and facilitate the reorganization of actin and myosin at the cleavage furrow, while in plants microtubules form the scaffold of a cell wall–generating structure at the plane of division, the phragmoplast (4).

A key regulator of microtubule organization is the multimember Aurora kinase family (5). Aurora activity is linked to a protein assembly called chromosomal passenger complex (CPC) at both the centromeres and at the site of cytokinesis. The CPC is best studied in animals and yeast where besides at least one of the Aurora paralogs it consists of three additional proteins: INCENP, Borealin, and Survivin, which interact via the formation of a three-helical bundle (6).

The localization of the CPC is highly dynamic during cell division and determines its function (6, 7). Before anaphase onset, the CPC localizes to the inner centromere, where it monitors interkinetochore tension and prevents chromosome missegregation. During anaphase, the complex moves to the spindle midzone to promote cytokinesis (Fig. 1*A*).

Multiple mechanisms have been shown to impinge on the correct localization of the CPC during mitosis. For instance, Borealin has been shown to confer a general affinity for nucleosomes required for chromosome association (8), but the CPC's enrichment at centromeres in metaphase is dependent on at least two additional, partially interconnected pathways (9). On the one hand, Borealin has been shown to interact with Shugoshin, which can bind the centromere-associated histone mark H2AT120^{ph} deposited by the spindle checkpoint kinase Bub1. On the other hand, Survivin binds via its

Author affiliations: [a]Graduate School of Science and Technology, Nara Institute of Science and Technology, Nara, 630-0192 Japan; [b]Faculty of Science and Engineering, Groningen Biomolecular Sciences and Biotechnology Institute, University of Groningen, 9747 AG Groningen, The Netherlands; [c]Department of Plant Biotechnology and Bioinformatics, Ghent University, 9052 Ghent, Belgium; [d]VIB Center for Plant Systems Biology, 9052 Ghent, Belgium; and [e]Department of Developmental Biology, Institute for Plant Sciences and Microbiology, University of Hamburg, 22609 Hamburg, Germany

Author contributions: S.K., E.C.T., M.H., and A.S. designed research; S.K., E.C.T., G.D.J., and N.D.W. performed research; S.K., E.C.T., G.D.J., and A.S. contributed new reagents/analytic tools; S.K., E.C.T., G.D.J., M.H., and A.S. analyzed data; and S.K., E.C.T., M.H., and A.S. wrote the paper.

The authors declare no competing interest.

This article is a PNAS Direct Submission.

[1]To whom correspondence may be addressed. Email: shini-komaki@bs.naist.jp or arp.schnittger@uni-hamburg.de.

This article contains supporting information online at http://www.pnas.org/lookup/suppl/doi:10.1073/pnas.2200108119/-/DCSupplemental.

Published October 13, 2022.

Baculovirus IAP Repeat (BIR) domain to phosphorylated threonine 3 in the tail of histone H3 ($H3T3^{ph}$) that becomes phosphorylated by the kinase Haspin (10–12). In addition, a recent study showed that Survivin is also able to bind Shugoshin at its N terminus, which structurally resembles the phosphorylated H3 tail (13). Since both interactions involve the same site of Survivin's BIR domain, they are considered mutually exclusive in accordance with the model of two spatially distinct CPC pools: a Bub1-dependent kinetochore-proximal centromere pool, involving interactions of Survivin and Borealin with Shugoshin, and a Haspin-dependent inner centromere pool entailing the $H3T3^{ph}$ Survivin contact (14–16). The translocation of the CPC to the spindle midzone is then mediated by MKLP2, a member of the kinesin-6 family, which directly binds to the three-helical bundle of the CPC (17).

Comparative genomics and molecular analyses have revealed that *Arabidopsis*, and likely all other plants, are also equipped with a CPC similar to those found in animal and fungal model systems, which contains AUR3, one of three Aurora kinase paralogs in plants, INCENP, and a plant ortholog of Borealin, called BOREALIN RELATED (BORR) (2, 18–20). Loss of CPC function leads to gametophytic and sporophytic (embryonic) lethality in *Arabidopsis*, underlining its key role in cell proliferation across the eukaryotic tree of life (18, 20). As seen in other eukaryotes, the plant CPC dynamically changes its subcellular localization throughout the cell cycle. It localizes to inner centromeres and prevents chromosome missegregation in early mitosis, and after anaphase onset it relocates to the center of the phragmoplast (20). Additionally, it was shown that plant Haspin phosphorylates histone H3 tails at threonine 3 and that this activity is needed to recruit AUR3 to the inner centromere (21–23). However, an ortholog of the $H3T3^{ph}$-reader Survivin, needed for concentration of the CPC at the inner centromere, has not been identified in plants or any other eukaryotic lineages outside animals and fungi (19) (Fig. 1*B*).

Notably, in animals, next to its role in the CPC, Survivin also controls programmed cell death as a member of the inhibitor of apoptosis (IAP) protein family which is characterized by the presence of one to several BIR domains (24, 25). However, neither the IAP protein family nor a bona fide BIR domain can be found in plants (26–28). Moreover, plants do not undergo apoptosis but display different mechanisms of programmed cell death instead (26–28).

In this study, we isolate BOREALIN-RELATED INTERACTOR 1 and 2 (BORI1 and 2) from *Arabidopsis* and provide molecular and biochemical evidence that both proteins redundantly act as Survivin-like proteins with respect to the Survivin function in the CPC. Notably, instead of a BIR domain, BORIs contain an FHA domain to bind to phosphorylated histones. Furthermore, we reveal through comparative genomics that the Survivin/BORI gene family is widely conserved among eukaryotes. The key characteristics of this gene family can be delineated to two functional domains with distinct evolutionary histories: 1) an ancient and conserved helix to make contact with the other subunits of the CPC and 2) one domain characterized by convergent molecular evolution to mediate the interaction with $H3T3^{ph}$ at the inner centromere.

Results

Identification of Borealin-Interacting Proteins in Plants. Previously, we identified and functionally characterized a plant homolog of Borealin, called BOREALIN RELATED (BORR). BORR acts together with INCENP, also known as WYRD in *Arabidopsis thaliana* (18), as the scaffold of the presumed equivalent of the CPC in plants (20). However, an ortholog of Survivin, the third essential scaffolding subunit of the CPC, has so far not been detected outside animals and fungi (Fig. 1*B*), raising the hypotheses that Survivin function was replaced and/or is not necessary in plants and other eukaryotic lineages (2, 19, 20).

To identify putative CPC-associated components in plants, we performed tandem affinity purification (TAP) followed by mass spectrometry (MS) using an *Arabidopsis* cell suspension culture expressing BORR with a CGS^{rhino} tag at its C terminus (29). The experiment was performed in duplicate and in both cases only one protein, At3g02400, passed all thresholds of the TAP evaluation pipeline and was subsequently named BOREALIN RELATED INTERACTOR 1 (BORI1). In addition, the known BORR interactor INCENP/WYRD was found in both experiments although each time only with one peptide, i.e., below the two-peptide cutoff of the standard evaluation pipeline (Dataset S1).

At3g02400 was previously described as FORKHEAD-ASSOCIATED DOMAIN PROTEIN 3 (FHA3) and found to bind in vitro to a promoter fragment of PEROXIN 11b (PEX11b), which encodes a peroxisome protein. It was also reported to be nuclear-localized and its overexpression resulted in reduced peroxisome number (30). Notably, the genome of *Arabidopsis* contains one close homolog to BORI1, At4g14490, which we named BORI2. Both BORI1 and 2 are characterized by an N-terminal FHA domain and a helical domain at the C terminus (Fig. 1 *C* and *D*). Forkhead-associated (FHA) domains are small protein modules shown to recognize different phospho-epitopes, with a preference for phosphothreonine. FHAs have been identified in both prokaryotes and eukaryotes in a diverse range of proteins such as kinases, phosphatases, RNA- and DNA-binding proteins, and metabolic enzymes (31–34).

To get hints on the putative function of the BORIs, we performed a phylogenetic analysis of the FHA domain of BORI1 and 2 (*SI Appendix*). We found that BORI1 and 2 originated by a duplication in the common ancestor of Brassicaceae (Fig. 1*D*) and that additional BORI orthologs can only be found in Archaeplastida among both chlorophytes and streptophytes, but not rhodophytes. BORI orthologs are specifically characterized by the presence of a conserved C-terminal helix (Fig. 1*D*). Using the presence of this domain, we could separate the FHA domain of BORI orthologs from its closest paralogous FHA domain, found in the PP2C phosphatase KAPP [kinase associated protein phosphatase (35)], which resulted from a duplication in the common ancestor of Viridiplantae (composed of chlorophytes and streptophytes). KAPP interacts with various receptor kinases and regulates local phosphorylation status of such receptors at the plasma membrane (36, 37). The closest outgroup to KAPP/BORI FHA domains contains deltaproteobacterial proteins, suggesting a potential lateral transfer of FHA proteins from these prokaryotic lineages to the ancestor of Viridiplantae. The function of these prokaryotic homologs, however, is unclear.

To further test and validate the interaction of both BORIs with BORR, we generated plants producing green fluorescent protein (GFP) fusion proteins of BORI1 and 2 (PRO_{BORI1}:*BORI1:GFP*, PRO_{BORI2}:*BORI2:GFP*; see below) and crossed them with plants expressing PRO_{BORR}:*BORR:RFP*. As a control, we combined the previously generated PRO_{BORR}:*BORR:RFP* plants with plants producing GFP alone (PRO_{35S}:*GFP*) (20, 38). After IP with GFP-Trap beads using protein extracts from

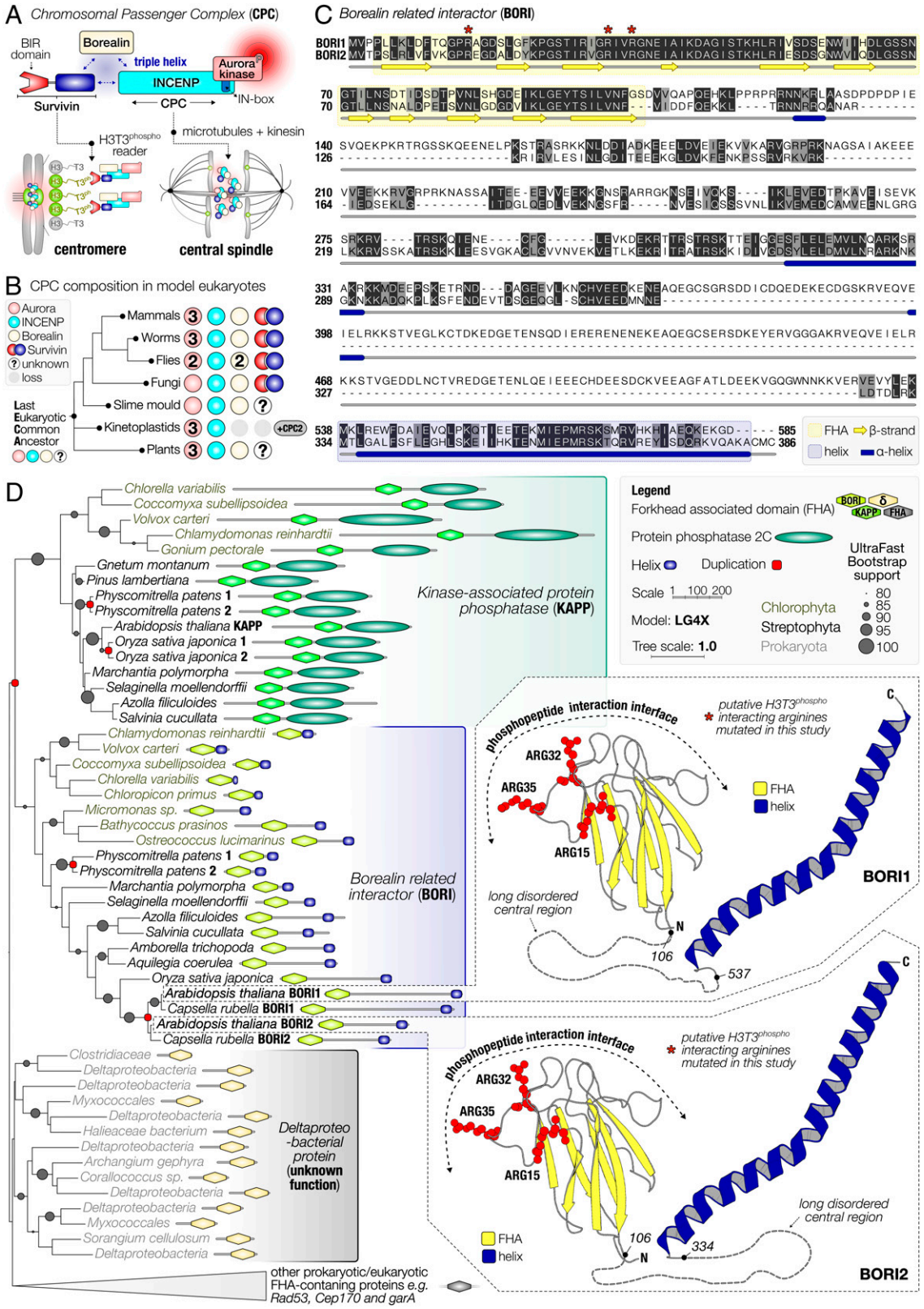

Fig. 1. *BOREALIN RELATED INTERACTOR* (*BORI*) genes in plants. (*A*) The CPC consists of an Aurora-type kinase scaffolded by the triple helix-based trimer INCENP, Borealin, and Survivin. Metaphase CPC localization at the centromere is dependent on a Survivin–H3T3^{ph} interaction and anaphase localization at the central spindle relies on interactions with microtubules and kinesins. (*B*) Presence–absence matrix of CPC components in model organisms that have previously been found throughout the eukaryotic tree of life (2, 19). Colors: similar to *A*. Numbers: paralog amount. Question mark: inability to detect orthologs. Gray circles: loss of components. (*C*) Multiple alignment of Borealin Related Interactor 1 and 2 found in *Arabidopsis thaliana*. FHA (yellow); C-terminal helix (dark blue). Secondary structure consensus of the Alphafold2 predicted 3D structures of BORI1-2 is projected below the alignment. Stars: three arginine residues (ARG-15-32-35), which likely face the phosphorylated histone H3 tail (see ball-and-sticks representation in *D*). Color scheme: 100% identity (black), similar physicochemical properties (gray), others (white). (*D*) Unrooted maximum-likelihood phylogenetic tree of FHA domains most similar to BORI orthologs in prokaryotes and eukaryotes. Branch lengths (scaled; number of substitutions per site). Circles: bootstrap support (1,000× replicates, only higher than 80% support shown). Red squares: duplication nodes. Right: AthaBORI1 and 2 Alphafold2-predicted 3D structures, with putative phosphate-interacting residues in ball-and-sticks representation (see also *C*). Colors: FHA (yellow); helix (blue). See Dataset S2 for full-length 3D structures. For phylogenetic analysis details see Dataset S3.

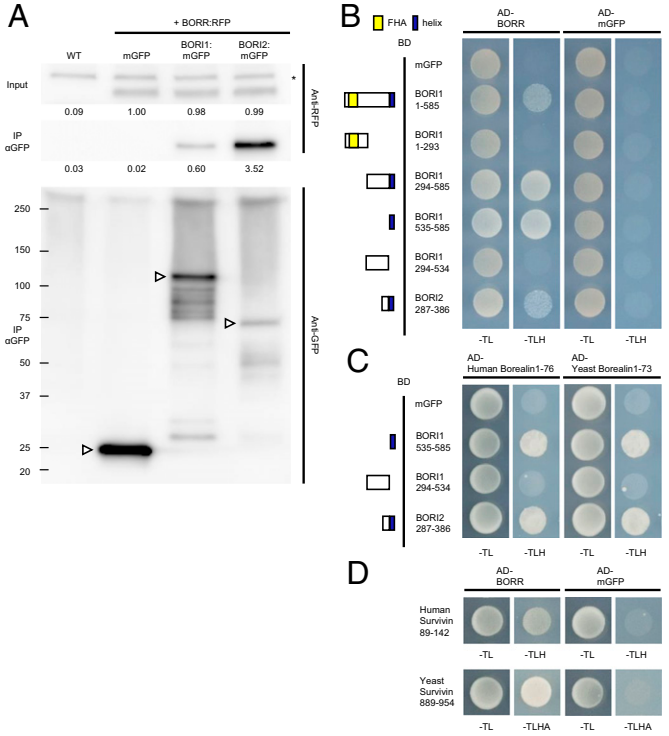

Fig. 2. Interaction between Survivin, BORIs, and BORR. (*A*) Co-IP of BORIs and BORR. Seven-day-old *Arabidopsis* seedlings expressing BORR:RFP and BORI1:mGFP or BORR:RFP and BORI2:mGFP were used for IP with an anti-GFP antibody. Both input and IP fractions were subjected to immunoblotting with an anti-RFP antibody to detect BORR:RFP. The relative intensity of the band signal (input fraction of mGFP = 1.00) is shown at the bottom. IP fractions were also subjected to immunoblotting with an anti-GFP antibody to detect GFP-tagged fusion proteins. Seedlings expressing both *BORR:RFP* and *mGFP* as well as wild-type (WT) seedlings were used as negative controls. The asterisk indicates a nonspecific band. Arrowheads indicate GFP-tagged fusion proteins. (*B–D*) Identification of the interaction domain between Survivin, BORIs, and BORR by yeast two-hybrid assay. Each strain was spotted on SD plates without Trp and Leu (−TL; control media) or without Trp, Leu, and His (−TLH; selection media) and photographed after incubation at 30 °C for 2 d (*B* and *D*) or for 3 d (*C*). AD, GAL4-activation domain. BD, GAL4-DNA binding domain. mGFP was used as a negative control.

seedlings, we detected complex formation between BORR:RFP and BORI1:GFP as well as BORR:RFP and BORI2:GFP but not between BORR:RFP and GFP alone (Fig. 2*A*).

To test for direct interaction and to subsequently map the interaction domains between BORR and the BORIs, we performed yeast two-hybrid assays. Deletion analyses revealed that the conserved C-terminal helix of the BORIs is necessary for the contact with BORR (Fig. 2*B* and *SI Appendix*, Fig. S1). Since this domain configuration is reminiscent of Survivin, which also interacts with Borealin via its C-terminal helix in the context of the three-helical bundle formed with INCENP (6), we speculated that the BORIs might be bona fide homologs of Survivin in plants by virtue of their C-terminal domains.

The FHA Domain of BORIs Specifically Binds Phosphorylated Histone H3 Threonine 3. In case of functional conservation, we hypothesized that BORI, like Survivin, should be able to bind to phosphorylated H3T3 presumably via its N-terminal FHA domain. Notably, the tails of histone H3 are highly conserved in the eukaryotic kingdom, including the two threonine residues (T) T3 and T11 as possible phosphorylation sites (Fig. 3*A* and *SI Appendix*, Fig. S2). To test for binding to histone H3, we first performed coimmunoprecipitation (co-IP) assays using protein extracts of transgenic *Arabidopsis* seedlings expressing PRO_{BORI1}:*BORI1:GFP* or PRO_{BORI2}:*BORI2:GFP*. Wild-type and PRO_{35S}:*GFP*-expressing plants were used as negative controls. After IP with GFP-Trap beads, we successfully detected histone H3 in BORI1:GFP and BORI2:GFP samples but not in the wild-type and GFP-alone samples (Fig. 3*B*). Next, we performed histone H3 peptide-binding assays to address whether BORIs can interact with phosphorylated histone H3 tails (Fig. 3*C*). Synthesized histone-H3 tails with or without a phosphate group at amino acid T3 and/or T11 were conjugated with biotin and incubated with the GST-fused FHA domain of BORI1 or BORI2. Human Survivin and GST alone were used as positive and negative controls, respectively. Bound proteins were retrieved using streptavidin-coupled magnetic beads and detected by Western blotting. As shown in Fig. 3 *C* and *D*, both FHA domains poorly bound to nonphosphorylated H3 peptides. Notably, the affinities to H3 peptides were strongly enhanced by $H3T3^{ph}$ but not $H3T11^{ph}$, indicating that the FHA domain of BORIs can specifically recognize the phosphorylation status of histone H3 at threonine 3 (Fig. 3 *C* and *D*).

According to different structures of FHA domains bound to phosphopeptides, arginine residues in the loops between the β-sheets of the FHA domain are often involved in direct contact with the phosphate residue of the phospohopeptide, including those found in the FHA domain of KAPP (39–42). Using the Alphafold2 three-dimensional (3D) predicted structures of BORI1 and 2 (*SI Appendix*, Dataset S2), we identified three arginine residues present in loops that are potentially facing the phosphorylated histone H3 (Fig. 1 *C* and *D*). We substituted all three arginine residues in these loops with alanine (Fig. 1*C*) with the aim to disturb $H3T3^{ph}$ binding. When tested in vitro, both

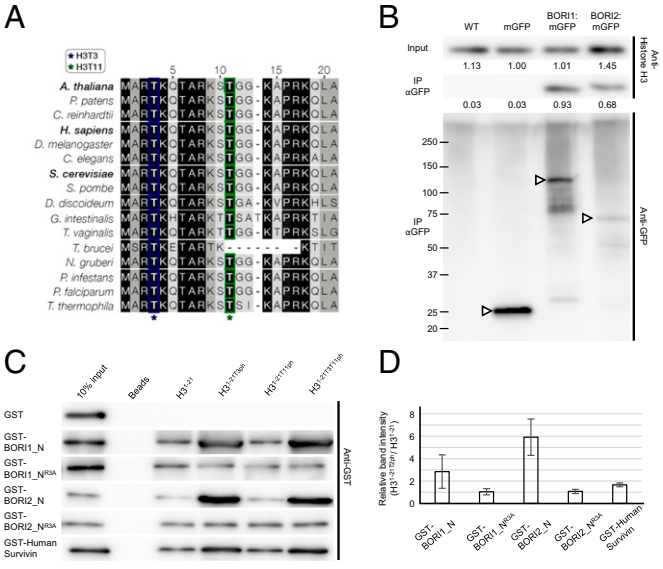

Fig. 3. The FHA domain of BORIs directly binds to $H3T3^{ph}$. (*A*) Multiple sequence alignment of the H3 N terminus in different species showing conservation of threonine 3 and 11 (T3, T11). Histone H3 polypeptides are typically numbered with omission of the N-terminal methionine, since it is likely removed cotranslationally (58, 59). Therefore, the initiator Met has not been included in the peptides used in the in vitro assays in *C*. (*B*) Co-IP of BORIs and Histone H3. Seven-day-old *Arabidopsis* seedlings expressing BORI1:mGFP or BORI2:mGFP were used for IP with an anti-GFP antibody. Both input and IP fractions were subjected to immunoblotting with an anti-Histone H3 antibody. Seedlings expressing mGFP and wild-type (WT) seedlings were used as negative controls. (*C*) Peptide-binding assay. All peptides were biotinylated at the C terminus and were preincubated with streptavidin-coated beads before addition of FHA domains. Protein binding was subjected to immunoblotting with an anti-GFP antibody. A GST-fusion of human Survivin and GST alone were used as positive and negative controls, respectively. (*D*) Relative band intensities comparing $H3^{1\text{-}21T3ph}$ and $H3^{1\text{-}21}$ in *B* were calculated. Data shown represent three independent experiments.

mutated FHA domains (R3A mutants) indeed showed drastically reduced H3T3^{ph}-binding affinities (Fig. 3*B*). Thus, although BORIs and Survivin have different histone H3-binding domains, their binding affinities to H3 peptides can be specifically enhanced by H3T3 phosphorylation.

BORIs Are Required for Proper Chromosome Segregation and Cell Division. For a functional analysis, we isolated a T-DNA insertion mutant of *BORI1* (*bori1-1*) that did not express full-length *BORI1* transcript (*SI Appendix*, Fig. S3 *A–C*). Since T-DNA insertion mutants for *BORI2* were not available, we generated a mutant by CRISPR/Cas9. The resulting *bori2-1* allele has an 8-bp deletion that creates a premature stop codon (*SI Appendix*, Fig. S3*A*). Since both single mutants showed no obvious mutant phenotypes, we combined *bori1* with *bori2* to overcome a possible functional redundancy. No difference in growth and fertility in comparison to the wild type were detected in plants which are homozygous mutant for one and heterozygous for the other *BORI* gene (*SI Appendix*, Fig. S4 *A–C*). However, double-homozygous mutants could not be recovered among more than 380 seedlings in the progeny of *bori1*$^{+/-}$ *bori2*$^{-/-}$ and *bori1*$^{-/-}$ *bori2*$^{+/-}$ plants. Instead, we observed aborted and undeveloped seeds in siliques of *bori1*$^{+/-}$ *bori2*$^{-/-}$ and *bori1*$^{-/-}$ *bori2*$^{+/-}$ (Fig. 4 *A* and *B*).

To confirm that the lethal phenotype was due to the mutated *BORI* genes, we carried out complementation tests using the two *BORI* genomic fragments, each fused with *GFP* (*PRO$_{BORI1}$:BORI1:GFP* and *PRO$_{BORI2}$:BORI2:GFP*; see above). Either construct could fully complement the lethal phenotype of the double-homozygous mutants, indicating that *BORI* function is essential in plants, similarly to the previously analyzed

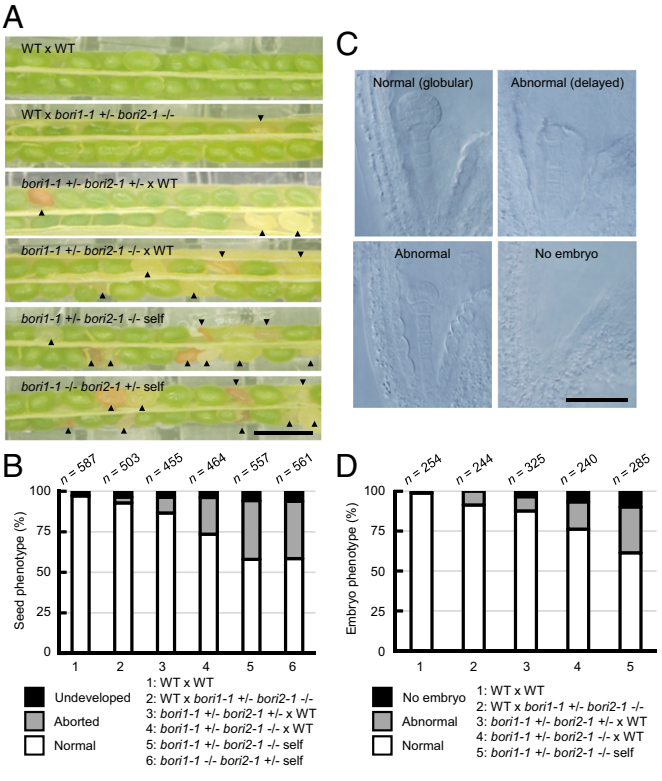

Fig. 4. Mutants in *BORI* exhibit defects in embryo development. (*A*) Developing seeds in a silique resulting from reciprocal crosses between *bori* mutants and the wild type (WT). Arrowheads indicate aborted seeds. (Scale bar, 1 cm.) (*B*) Frequency of seed phenotypes shown in each cross. (*C*) Embryo phenotypes observed in *bori* mutants. Whole-mount clearing was conducted 4 d after the pollination. (Scale bar, 100 μm.) (*D*) Frequency of embryo phenotypes shown in each cross.

other two components of the CPC (*SI Appendix*, Fig. S4 *A–C*) (18, 20).

Since we observed more than 25% aborted and/or undeveloped seeds as well as more than 25% seeds with an abnormal embryo or no embryo (Fig. 4 *B* and *D*), we performed a reciprocal cross between *bori1*$^{+/-}$ *bori2*$^{-/-}$ and wild-type plants to examine the transmission efficiency of the *bori1* allele as a proxy for developmental defects of the mutant gametophytes. When we used *bori1*$^{+/-}$ *bori2*$^{-/-}$ as the male parent, the transmission efficiency was only slightly reduced to 94.2% ($n = 200$). In contrast, when we used *bori1*$^{+/-}$ *bori2*$^{-/-}$ as the female parent, the transmission efficiency dropped to 38.9% ($n = 200$), indicating that BORIs have an important role in the function and/or development of the female gametophyte. However, when analyzing mature siliques, we rarely observed unfertilized ovules, indicating that the reduction of the transmission efficiency manifested only after fertilization during embryo development (Fig. 4 *A* and *B*). Consistently, we frequently found abnormal embryo development when *bori1*$^{+/-}$ *bori2*$^{-/-}$ was used as the female parent and pollinated with wild-type pollen (Fig. 4 *C* and *D*). Since we still observed aborted and undeveloped seeds when double-heterozygous *bori1*$^{+/-}$ *bori2*$^{+/-}$ mutant plants as the female parent were pollinated with wild-type pollen, we conclude that the lethal phenotype does most likely not arise from a maternal sporophytic effect but indeed from an alteration of female gametophyte development (Fig. 4 *A–D*).

To study the possible *BORI* function after embryogenesis, we constructed an artificial microRNA against *BORI2* (*amiBORI2*) and transformed it into *bori1-1*$^{-/-}$ mutants. Most of the transformants (15 of 18) exhibited a dwarf phenotype. We selected four transformants that showed different reduction levels of *BORI2* transcript for further analysis (*amiBORI2#1*^{bori1}, *amiBORI2#2*^{bori1}, *amiBORI2#3*^{bori1}, and *amiBORI2#4* ^{bori1}) (*SI Appendix*, Fig. S3*D*). A dose-dependent reduction in leaf area and curling of leaves were observed for these *amiBORI* mutants (*SI Appendix*, Fig. S4*A*). As found in *BORR* knockdown mutants, the reduction of *BORI* transcript levels also resulted in plants displaying the so-called *bonsai* phenotype with compact inflorescences at flowering stage (*SI Appendix*, Fig. S4 *B* and *C*). To further test whether compromised CPC function gives rise to a *bonsai* phenotype, we also generated plants expressing a microRNA against AUR3 (*SI Appendix*, Fig. S3*E*). Indeed, *AUR3* knockdown plants revealed the same phenotype as *amiBORR* and *amiBORI* mutant plants (*SI Appendix*, Fig. S4 *A–C*).

The growth of primary roots was also compromised by the knockdown of *BORI2* in *bori1* mutants (Fig. 5 *A* and *B*). We observed that many cells died in the root meristems of *amiBORI* mutant plants (Fig. 5 *C* and *D*). In addition, *amiBORI* mutants produced root meristems of reduced size and with aberrant cell divisions (Fig. 5 *C*, *E*, and *F*). We have previously shown that impaired CPC activity in plants causes chromosome segregation defects, for instance lagging chromosomes in anaphase, consistent with compromised CPC activity in animals and yeast (20). To monitor possible mitotic defects, we crossed the *amiBORI2#2*^{bori1} and *amiBORI2#3*^{bori1} mutants with a previously generated transgenic line expressing both a microtubule (*RFP:TUA5*) and a centromere (*GFP:CENH3*) marker (38). Analysis of the resulting plants revealed that both *amiBORI2#2*^{bori1} and *amiBORI2#3*^{bori1} mutants also have lagging chromosomes and the frequency of these segregation defects increased with the level of *BORI* transcript reduction (Fig. 5 *G* and *H*). Thus, loss of BORI function results in aneuploidy and likely in the further course of development, secondary

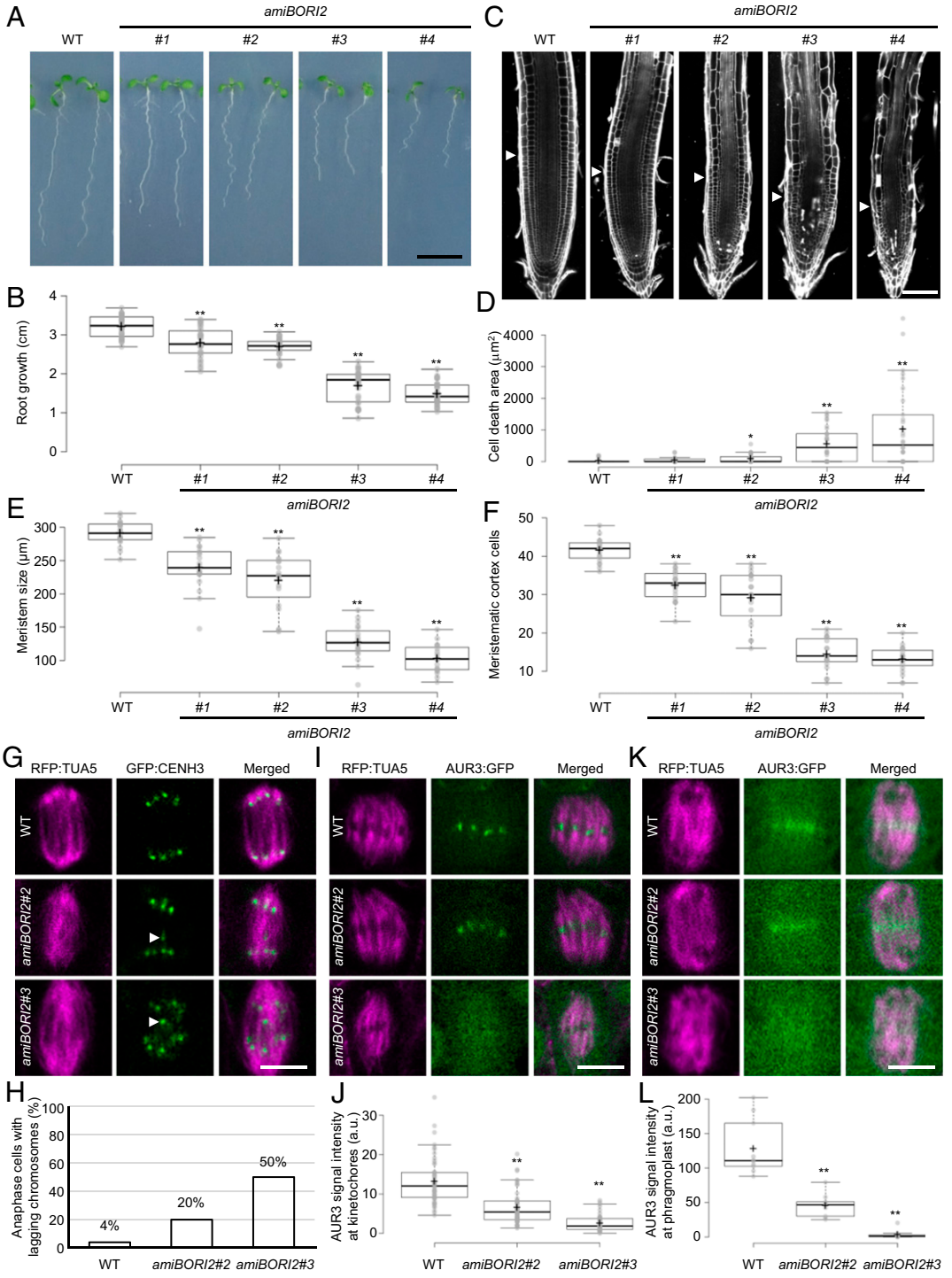

Fig. 5. Phenotypic analysis of amiRNA-mediated *BORI* knockdown plants. (*A*) Seven-day-old wild-type (WT) and *BORI* knockdown seedlings. (Scale bar, 1 cm.) (*B*) Root length of 7-d-old WT and *BORI* knockdown seedlings. Graph bars represent means ± SD. Asterisks indicate significant difference between the WT and *BORI* knockdown seedlings tested by Student's *t* test (**$P < 0.001$, $n = 30$). (*C*) Confocal images of 7-d-old WT and *BORI* knockdown roots stained with 20 μg/mL propidium iodide to visualize cell walls and dead cells. Arrowheads indicate the boundary between the division region and the elongation region of the root. (Scale bar, 100 μm.) (*D*) Cell death area in *C*. Asterisks indicate significant difference between WT and *BORI* knockdown seedlings tested by Student's *t* test (*$P < 0.01$, **$P < 0.001$, $n = 20$). (*E*) Meristem size in *C*. Meristem size was measured from quiescent center to the first elongated cell in the cortical cell file. Asterisks indicate significant difference between WT and *BORI* knockdown seedlings tested by Student's *t* test (**$P < 0.001$, $n = 20$). (*F*) Number of meristematic cortex cells in *C*. Asterisks indicate significant difference between WT and *BORI* knockdown seedlings tested by Student's *t* test (**$P < 0.001$, $n = 20$). (*G*) Representative images of normally distributed and lagging chromosomes in 5-d-old WT and *BORI* knockdown roots. Microtubules and centromeres were visualized by RFP:TUA5 and GFP:CENH3, respectively. Arrowheads indicate lagging chromosomes. (Scale bar, 5 μm.) (*H*) Frequency of lagging chromosomes in anaphase cells in *G*. $n = 50$. (*I*) Representative images of AUR3 accumulation levels at metaphase centromeres in 5-d-old WT and *BORI* knockdown roots. Microtubules and AUR3 were visualized by RFP:TUA5 and AUR3:GFP, respectively. (Scale bar, 5 μm.) (*J*) AUR3 signal intensity in *I*. AUR3:GFP signals at metaphase centromeres were measured. Asterisks indicate significant difference between WT and *BORI* knockdown roots tested by Student's *t* test (**$P < 0.001$, $n = 50$). (*K*) Representative images of AUR3 accumulation levels at the middle part of the phragmoplast in 5-d-old WT and *BORI* knockdown roots. Microtubules and AUR3 were visualized by RFP:TUA5 and AUR3:GFP, respectively. (Scale bar, 5 μm.) (*L*) AUR3 signal intensity in *K*. AUR3:GFP signals at the middle part of the phragmoplast were measured. Asterisks indicate significant difference between WT and *BORI* knockdown roots tested by Student's *t* test (**$P < 0.001$, $n = 10$).

developmental defects and cell death. This finding also could explain the severe embryonic versus rather mild gametophytic defects described above since aneuploidy arisen during gametophyte development might cause embryo abortion only after a few divisions of the zygote.

To address whether the *BORI* loss-of-function phenotype was due to mislocalization of AUR3, we investigated the AUR3 accumulation at centromeres and phragmoplast by introducing a PRO_{AUR3}*:AUR3:GFP* reporter (20) into *amiBORI2*^{bori1} plants. Indeed, abundance of AUR3 at centromeres and phragmoplast was drastically reduced in both *amiBORI2#2*^{bori} and *amiBORI2#3*^{bori1} mutants, indicating that BORIs are required for proper localization of the CPC complex (Fig. 5 *I–L*).

BORIs Are Needed for Proper Targeting of the CPC to Chromatin In Vivo. Transient expression of the *BORI1* complementary DNA (cDNA) fused to the open reading frame of GFP under the control of the constitutive *Cauliflower mosaic virus promoter 35S* was previously found to result in homogeneous accumulation of the fusion protein in the nucleoplasm of mature tobacco leaves (30). To investigate the detailed subcellular localization of BORIs during cell proliferation, we combined each of our genomic *BORI:GFP* reporters with a *RFP:TUA5* marker line and analyzed their coexpression pattern in *Arabidopsis* root tips. BORI1:GFP and BORI2:GFP showed the same localization pattern throughout the cell cycle (Fig. 6*A*, *SI Appendix*, Fig. S5*A*, and Movies S1 and S2) and thus will be described in the following as BORI:GFP. In interphase, BORI:GFP localized to the nucleoplasm and accumulated in nuclear foci. Colocalization analyses with *RFP:CENH3* revealed that these foci are centromeres. Since CENH3 marks the kinetochore-proximal centromeres, we further concluded that BORI:GFP resides at inner centromeres similar to the other CPC components (*SI Appendix*, Fig. S5*G*) (20).

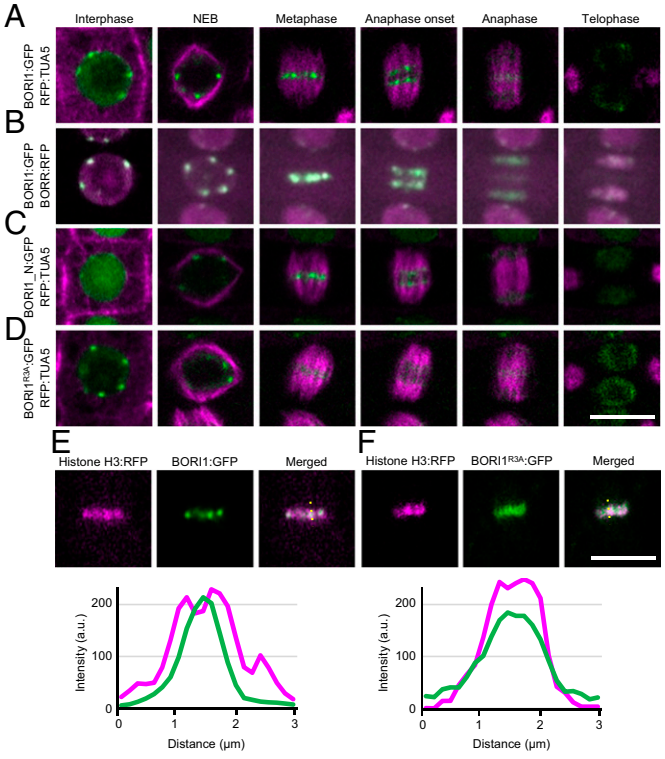

Fig. 6. Subcellular localization of BORI1 during the cell cycle. (*A*) Subcellular localization of BORI1:GFP during the cell cycle. Microtubule structures were visualized by RFP:TUA5. (*B*) Colocalization of BORI1:GFP and BORR:RFP. (*C* and *D*) Subcellular localization of BORI1_N:GFP (*C*) or BORI1^{R3A}:GFP (*D*) during the cell cycle. Microtubule structures were visualized by RFP:TUA5. For live imaging, root tips of 5-d-old seedlings were used. (Scale bar, 10 μm.) (*E* and *F*) Colocalization of Histone H3:RFP and BORI1:GFP (*E*) or BORI1^{R3A}:GFP (*F*) in metaphase cells. The yellow dotted line indicates the positions where the line profiles were obtained. (Scale bar, 10 μm.).

In mitotic cells, the BORI:GFP signal rapidly concentrated at the centromeres starting just after nuclear envelope breakdown until metaphase. After anaphase onset, BORI:GFP changed its localization from centromeres to the center of phragmoplasts (*SI Appendix*, Fig. S5*D*), and, after completion of cell division, BORI:GFP reaccumulated in the nucleus. The localization pattern of BORI:GFP completely overlapped with that of BORR:RFP throughout the cell cycle (Fig. 6*B* and Movie S3).

To understand the spatial regulation of BORI during the cell cycle, we generated a BORI1:GFP reporter driven by its own promoter but without the BORR-interacting helix at the C terminus of the protein (amino acids 1 to 293: PRO_{BORI1}*:BORI1_N:GFP*). BORI1_N:GFP accumulated at centromeres from prophase to metaphase similar to the full-length BORI1-GFP. However, BORI1_N:GFP signals were only detected on chromosomes and not at the phragmoplast in late anaphase (Fig. 6*C*, *SI Appendix*, Fig. S5*F*, and Movie S4). To test whether the aberrant localization of BORI1_N:GFP at the phragmoplast was caused by the failure to interact with BORR, we crossed the wild-type BORI1:GFP reporter with previously *amiBORR* mutant (*SI Appendix*, Fig. S3*F*) (20). Indeed, BORI1:GFP did not localize to the phragmoplast in *amiBORR* mutants (*SI Appendix*, Fig. S5 *C* and *E* and Movie S5), corroborating that the interaction of BORIs with BORR is necessary for the targeting of BORIs to phragmoplasts but not to centromeres.

In other organisms, Survivin concentration at inner centromeres relies on the phosphorylation of histone H3 at threonine 3 (H3T3^{ph}) catalyzed by Haspin. To check whether H3T3^{ph} is required for BORI localization to centromeres, *BORI1:GFP* plants were treated with the Haspin inhibitor 5-Iodotubercidin (5-ITu) (22, 43). Although we could still detect BORI1:GFP at centromeres after treatment, the GFP signal in metaphase was much more diffuse (*SI Appendix*, Fig. S5*H*). Notably, we could reproduce the same localization defect by introducing the R3A substitution into *BORI:GFP* (*BORI*^{R3A}*:GFP*) that reduces the binding affinity to H3T3^{ph} (see above) (Fig. 6*D*, *SI Appendix*, Fig. S5*B*, and Movies S6 and S7). To analyze the localization of BORI^{R3A}:GFP in detail, we created transgenic plants that expressed a Histone H3 marker (Histone H3:RFP) together with BORI:GFP or BORI^{R3A}:GFP. Whereas BORI:GFP only colocalized with Histone H3:RFP at the inner region of the centromere, BORI^{R3A}:GFP localized to the entire Histone H3:RFP-marked region (Fig. 6 *E* and *F* and *SI Appendix*, Fig. S5 *I* and *J*). These results demonstrate that the binding of BORIs to H3T3^{ph}, similar to Survivin in animals and yeast, is crucial for their accumulation at the inner centromere.

To address the functional relevance of the precisely targeted centromere localization of BORIs, we expressed the *BORI1*^{R3A}*:GFP* construct in *bori1 bori2* double-homozygous mutants. While the *BORI1*^{R3A}*:GFP* construct could complement the lethal phenotype of the double-homozygous mutants, the resulting plants exhibited a wide range of developmental defects (Fig. 7 *A* and *B* and *SI Appendix*, Fig. S4 *D–F*). Foremost, these plants displayed severe growth defects and, as observed in *BORI* knockdown plants, the *BORI1*^{R3A}*:GFP*-expressing plants also contained many dying cells in their root meristems, possibly caused by aneuploidy (Fig. 7 *C* and *D*). Indeed, we observed chromosomal variations in *BORI1*^{R3A}*:GFP*-expressing root cells that contained between 8 and 11 chromosomes in contrast to the invariable 10 chromosomes found in the wild type (Fig. 7 *E* and *F* and Movies S8–S10). These

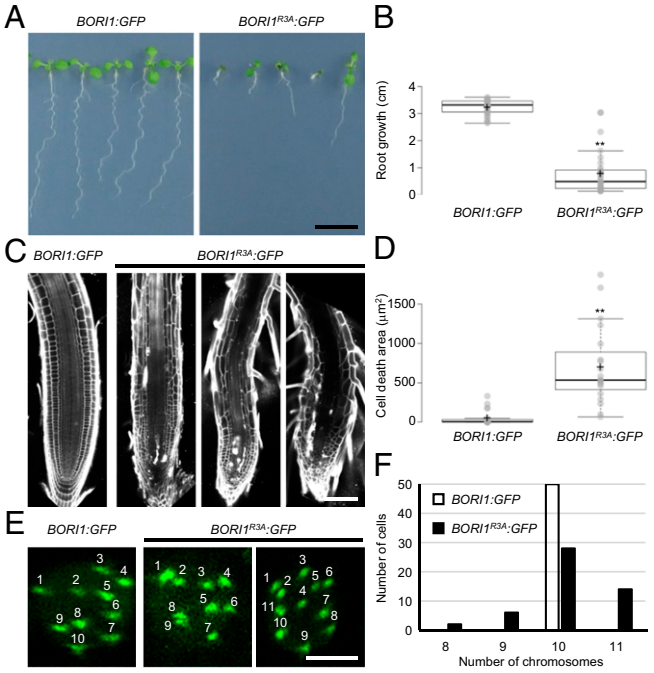

Fig. 7. Proper centromere localization of BORIs is required for genome stability. (*A*) Seven-day-old transgenic lines expressing *BORI1:GFP* or *BORI1^{R3A}:GFP* in *bori1 bori2*. (Scale bar, 1 cm.) (*B*) Root length of 7-d-old transgenic seedlings. Graph bars represent means ± SD. Asterisks indicate significant difference tested by Student's *t* test (**$P < 0.001$, $n = 30$). (*C*) Confocal images of 7-d-old *BORI1:GFP* and *BORI1^{R3A}:GFP* seedling roots stained with 20 µg/mL propidium iodide to visualize cell walls and dead cells. (Scale bar, 100 µm.) (*D*) Cell death area in *C*. Asterisks indicate significant difference tested by Student's *t* test (**$P < 0.001$, $n = 20$). (*E*) GFP signals in interphase cells of *BORI1:GFP* and *BORI1^{R3A}:GFP* seedling roots. (Scale bar, 5 µm.) (*F*) Number of chromosomes in interphase cells of *BORI1:GFP* and *BORI1^{R3A}:GFP* seedling roots ($n = 50$).

results demonstrate that proper centromere localization of BORIs, which is mediated by their recognition of H3T3^{ph}, is required for genome stability.

The Defining Feature of the Survivin/BORI Gene Family Is a Coiled-Coil–Forming Helix. Since we found that the BORIs resembled Survivins with respect to their function in the CPC, and that both genes harbor a C-terminal conserved helix, we wondered whether human and yeast Borealin could bind to BORIs and, conversely, whether the helix of both human and yeast Survivin could directly interact with BORR from *Arabidopsis*. Indeed, we found in Y2H experiments heterologous interaction between the human/yeast and *Arabidopsis* proteins and domains (Fig. 2 *C* and *D*).

Given the interaction of BORI/Survivin with Borealin orthologs of different species, we next asked whether the C-terminal helices of BORI and Survivin would show significant sequence/structure similarity indicative of a common descent. We first constructed hidden Markov models (HMMs), using the *Arabidopsis* BORI C-terminal helices as a template. Following iterative searches in large eukaryotic sequence databases we (re)trained our HMM and could identify bona fide animal and fungal Survivin homologs (*SI Appendix*, *Supplementary Methods*). This strategy also worked in a reciprocal fashion, i.e., when searches were initiated with the helix of animal Survivin homologs, we were able to identify plant BORI homologs.

Such reciprocal similarity connections together with our above-presented functional analyses strongly suggests that the helices of Survivin and BORIs are orthologous, placing all these proteins bearing a helix into the same gene family. In contrast, the BIR/FHA domain should be considered accessory, giving rise to a hybrid nature of Survivin and BORI proteins with an ancient and conserved helical domain and an independently acquired and analogous chromatin binding domain.

Excitingly, using our helix-specific HMM strategy, we identified Survivin/BORI-type proteins in all eukaryotic supergroups (Fig. 8 A and B), in contrast to earlier attempts, which concentrated on the BIR domain of animal and fungal Survivins (19). We detected Survivin/BORI-type proteins with four different domain topologies in different eukaryotic (super)groups (Fig. 8 *A*–*D*): 1) Fungi and Metazoa harbor Survivin with 1 or 2 N-terminal BIR domains and a C-terminal helix, 2) Viridiplantae have an N-terminal FHA domain and a C-terminal helix, 3) Stramenopila and Haptista share a reversed topology with an FHA domain at the C terminus following the conserved helix, and 4) Amoebozoa, Rhodophyta, Discoba, Cryptista, and Metamonada contain relatively short homologs, with a single helix and no additional recognizable domains.

To determine the evolutionary history of the FHA domain of BORI-like proteins found in Stramenopila and Haptista, relative to those found in Viridiplantae BORIs, we performed a phylogenetic analysis (*SI Appendix*). We found that both FHA subtypes are more closely related to different FHA domains found in Deltaproteobacteria than to each other (Fig. 8*C*). Such phylogenetic relationships indicate an ancient lateral transfer of prokaryotic FHA domains to at least two ancient eukaryotic ancestral lineages, suggesting a distinct, but ancient, prokaryotic evolutionary origin for the FHA domain found in BORI-like proteins of Viridiplantae as well as Stramenopila and Haptista.

These results point to an evolutionary scenario for the Survivin/BORI gene family in which the ancestral version present in the last eukaryotic common ancestor (LECA) only consisted of a helix contributing to the triple helix structure of the CPC scaffold. The acquisition of a phosphate-binding domain occurred independently in at least three different clades, resulting in molecular convergence between Survivin in Fungi and Metazoa (+N-terminal BIR), BORI-like orthologs in Viridiplantae (+N-terminal FHA), and Stramenopila and Haptista (+C-terminal FHA) with respect to their capacity to bind phosphorylated H3T3 (Fig. 8*D*).

Discussion

Here, we have presented the identification of BORI1 and 2, two BORR-interacting proteins, that execute the Survivin function in the CPC of *Arabidopsis* in a redundant fashion. The BORIs belong to a Viridiplantae-specific protein family with members of variable size that consists of an N-terminal FHA domain and a conserved C-terminal helix with a propensity to form a coiled-coil (triple-helix) structure. We demonstrate that the FHA domain of BORIs act as a H3T3^{ph} reader at inner centromeres, a function fulfilled by the BIR domain in animals and yeast. Although both domains are capable of binding H3T3^{ph}, they are structurally very different. The FHA domain consists of a sandwich of β-sheets while the BIR domain displays three short alpha-helices and is stabilized by a zinc molecule, tetrahedrally coordinated by one histidine and three cysteine residues. Thus, there is no evidence of a common evolutionary history of the two domains. In contrast, the C terminus of the BORIs, which we showed here to interact with BORR, has residual sequence similarity with the helical domain of Survivin in animals and yeast as found by reciprocal HMM searches indicating a common ancestor.

Interestingly, the HMM searches based on the conserved helix also led to the discovery of Survivin/BORI-type proteins in additional phylogenetic groups which either display the helix as the

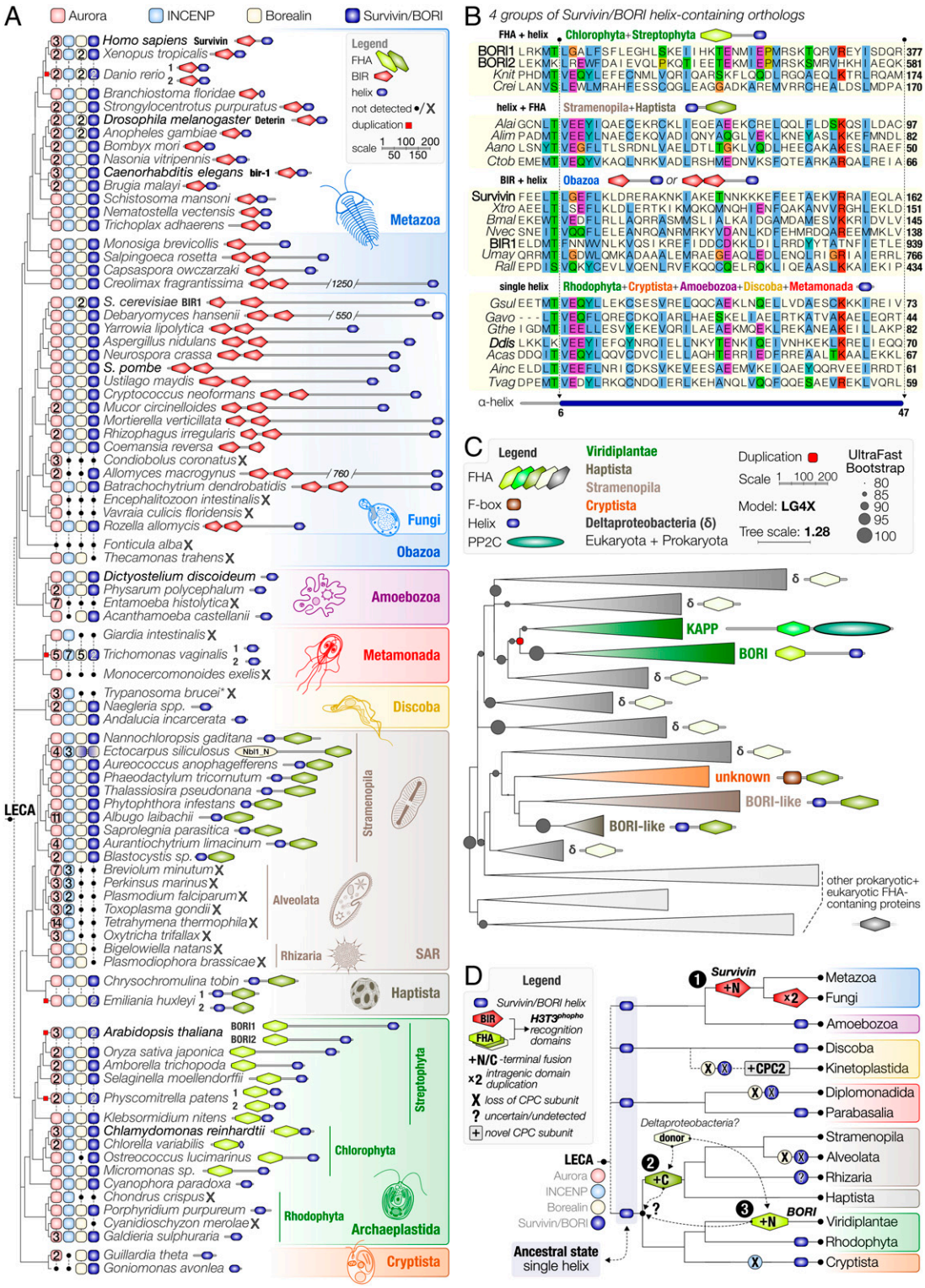

Fig. 8. A conserved helix and the recurrent acquisition of a phosphate-binding domain characterize the divergent Survivin/*BORI* gene family. (*A*) Presence–absence matrix of the four subunits of the CPC: Aurora kinase, INCENP, Borealin, and Survivin/BORI found across different eukaryotic supergroups [according to Burki et al. (60)]. Dashed lines indicate uncertain relationships among supergroups. LECA refers to the position of the last eukaryotic common ancestor. Numbers indicate paralog count. Domain topologies for Survivin/BORI on the right, with a conserved helix (blue) as the defining feature of this gene family. Different colored FHA domains indicate a unique evolutionary origin found in Survivin/BORI orthologs in different eukaryotes. (*B*) Multiple alignment of a conserved helix found in four subtypes of Survivin/BORI orthologs. Four-letter abbreviations refer to species that can be found in *A*. Numbers on the right indicate the position of the C terminus of a 47-residue-long helix. (*C*) Collapsed and unrooted maximum-likelihood phylogenetic tree of eukaryotic and prokaryotic FHA domains most similar to BORI, and Survivin/BORI-like proteins found among Archaeplastida, SAR, and Haptista. Representative domains for each collapsed clade are projected. Branch lengths are scaled (number of substitutions per site). Circles indicate bootstrap support (1,000× replicates, only higher than 80% support shown). Colors indicate diverse evolutionary histories of various domains (e.g., FHA of KAPPs and BORIs). For phylogenetic analysis details see Dataset S4. (*D*) Evolutionary scenario of the Survivin/*BORI* gene family. An helix-only Survivin/BORI was present in LECA and independently fused to a phosphate-binding domain at least three different times during eukaryotic evolution, in the ancestors of Fungi and Metazoa (1:BIR), SAR and Haptista (2:C-terminal FHA), and Viridiplantae (3:N-terminal FHA). FHA domains were laterally transferred from Deltaproteobacteria. Colors are similar to *A* and *C*.

only defined structure in a relatively short protein or the helix plus an FHA-domain at the C-terminal end of the protein (Fig. 8). Based on this, we propose an evolutionary scenario in which the LECA possessed a helix-only version of Survivin to tether the three structural components of the CPC together. Then, in a process of convergent evolution different H3T3^{ph}-binding domains were recruited in the different branches of the eukaryotic domain, likely to optimize and focus CPC localization at the inner centromere. Since several mechanisms contribute to the defined centromere localization of the CPC during mitosis in animals, it is possible that these were added in a stepwise manner. It would be plausible, for example, that binding of the ancestral CPC to centromeres was originally mediated by Borealin interacting with nucleosomes in general and centromere-localized Shugoshin in particular, and that binding to H3T3^{ph} was only added later to optimize the localization or enhance the concentration of the CPC. Consistently, when we disturbed H3T3^{ph} binding by point mutations in the FHA domain, BORI localization to chromosomes was weaker and not confined to the centromere region in comparison to the nonmutated version, but not completely lost. Notably, the mutant phenotype of *bori1 bori2* double mutants expressing the *BORI1^{R3A}:GFP* construct is also less severe than for a null mutant in any of the CPC components and rather resembled the effect of expressing a BORI–RNA interference construct. However, although H3T3^{ph} binding by Survivin-type proteins is not the only pathway for centromere localization, the fact that we observe convergent molecular evolution in animals and plants, and possibly also in Stramenopila and Haptista, where an FHA domain has been added at the C terminus, suggests that binding to H3T3^{ph} is a very efficient way to concentrate the CPC at the centromeres.

The plant CPC relocates from the inner centromere to the middle part of the phragmoplast at anaphase, resembling the situation in animals where the CPC moves from centromeres to the spindle midzone (also known as central spindle) (17). Although the phragmoplast is a plant-specific microtubule structure, it shares several properties with the spindle midzone in animals, i.e., they both define the division plane and are composed of antiparallel microtubules. Thus, CPC function in the early phragmoplast in plants might be analogous to CPC function at the spindle midzone.

In animals, the relocation of the CPC in anaphase is presumably dependent on the mitotic kinesin MKLP2, a member of the kinesin-6 family (17). A recent study indicates that MKLP2 directly binds to the scaffold proteins of the CPC and transports the CPC along microtubules to the spindle midzone (44, 45). Notably, we observed that BORIs also rely on the Borealin-interacting domain for their phragmoplast localization at anaphase. Since many kinesins, including for example NACK1/2, POK1/2, and AtPAKRP1/1L, have been found to accumulate in the middle part of the phragmoplast, it is tempting to speculate that one of these kinesins contributes to the CPC relocation in plants.

Taken together, our characterization of BORIs in *Arabidopsis* led to a redefinition of the minimal architectural requirement for Survivin-type proteins in the context of the CPC, allowing for the identification of putative orthologs in most eukaryotic clades. The here-described case of molecular convergence by differential domain recruitment indicates that we need to broaden our search algorithms in the hunt for orthologs to incorporate such possibilities and to be more mindful of short helices/motifs as the basis for defining a gene family. Our analyses furthermore illustrate an example for the contribution of deltaproteobacterial genes to the origin of eukaryotic pathways, lateral gene transfers that have gained increasing interest in recent work (46, 47).

Our findings also indicate flexibility in the molecular solutions for concentrating the CPC at centromeres in (pro)metaphase found among different eukaryotic lineages. These patterns of flexibility and recurrent changes are reminiscent of the rapid molecular evolution often observed for kinetochore and centromere-proximal proteins (19). Such a situation can be well explained by the paradoxical evolutionary arms race between centromeric DNA and its directly interacting proteins caused by asymmetric meiosis in most eukaryotes, also known as the centromere drive hypothesis (48). Recent work on the mechanisms of centromere drive in mice indeed points toward a delicate balance between regulation of the kinetochore superstructure and the (peri)centromeric chromatin environment, to which Aurora kinase activity has broad regulatory input (49, 50). The patterns of recurrent evolution of the Survivin/*BORI* gene family facilitating the differential recruitment of the CPC to chromatin that we find in our study might thus hallmark evolutionary events that fuel the ongoing war between overzealous centromeres and kinetochores in ancestral eukaryotic lineages.

Materials and Methods

Detailed descriptions of the methodology and data for this study are provided in *SI Appendix, Supplementary Methods*.

Plant Materials and Growth Conditions. The *Arabidopsis* (*A. thaliana*) accession Columbia (Col-0) was used as the wild type in this study. All mutants are in the Col-0 background. Plants were grown on a solid medium containing half-strength Murashige and Skoog salts, 1% (wt/vol) sucrose, and 1.5% (wt/vol) agar in a growth chamber at 22 °C (16 h of light/8 h of dark). The T-DNA insertion line SALK_095831 (*bori1-1*) was obtained from the Nottingham *Arabidopsis* Stock Center. The *bori2-1* line was generated by CRISPR/cas9. Primer pairs for genotyping are described in *SI Appendix*, Table S1 and Fig. S1 *A–C*.

TAP. Cloning of the transgene encoding a C-terminal GSrhino tag fusion under control of the constitutive cauliflower tobacco mosaic virus 35S promoter and transformation of *Arabidopsis* cell suspension cultures (PSB-D) was carried out as previously described (29, 51). TAP experiments were performed with 100 mg of total protein extract as input as described in Van Leene et al. (29). For details on liquid chromatography–MS/MS and data analysis see Dataset S1.

Plasmid Construction. The *BORI:GFP* reporter constructs, the CRISPR/cas9 construct against the *BORI2* gene, the amiRNA construct against *BORI2*, and the construct for BORI protein production were generated by PCR as detailed in *SI Appendix, Supplementary Methods* using the primer pairs listed in *SI Appendix*, Table S1.

Production of Recombinant BORI Proteins. Proteins were expressed in the *Escherichia coli* strain BL21 (DE3) harboring *pGEX6p-GW* containing the *BORI1* and *BORI2* cDNAs. Production was induced with 0.1 mM isopropyl β-D-1-thiogalactopyranoside at 16 °C for 16 h. Recombinant proteins were purified by affinity chromatography using Glutathione Sepharose 4B (cytiva) and stored at −80 °C.

Peptide-Binding Assay. H3$^{1-21}$ and H3$^{1-21T3ph}$ peptides were purchased from AnaSpec, Inc. H3$^{1-21T11ph}$ and H3$^{1-21T3T11ph}$ peptides were synthesized using SCRUM Inc. All peptides were biotinylated at the C terminus. For the peptide-binding assays, 40 pmol protein was incubated with 500 pmol peptide in 200 μL binding buffer (50 mM Tris·HCl, pH 7.5, 150 mM NaCl, 0.1% Nonidet P-40) with 0.25% (wt/vol) bovine serum albumin (BSA) at 4 °C for 3 h. Streptavidin-coated magnetic beads (Dynabeads M-280; Thermo Fisher Scientific) were preequilibrated in binding buffer with 0.25% (wt/vol) BSA. Thirty-microliter beads were added per assay and incubated at 4 °C for 1 h. Beads were washed three times with binding buffer and proteins were eluted by boiling in sodium dodecyl sulfate (SDS) loading buffer. Protein samples were analyzed by SDS polyacrylamide gel electrophoresis followed by Western blotting using 1:2,000 diluted anti-GST (Proteintech Group, Inc.) and 1:10,000 diluted anti-rabbit immunoglobulin G (IgG), horseradish peroxidase (HRP)-linked secondary antibody (cytiva).

Yeast Two-Hybrid Assay. Yeast two-hybrid assays were performed as described in ref. 38. Primer pairs for plasmid construction are described in *SI Appendix*, Table S1.

Microscopy. Ovules at 4 d after pollination were dissected from siliques and cleared with Herr's solution:lactic acid:chloral hydrate:phenol:clove oil:-xylene (2:2:2:2:1, wt/wt) and observed by OLYMPUS BX52 microscopy with differential interference contrast optics. For live-cell imaging, root tips of 5-d-old seedlings were used. Sample preparation and imaging were performed as described (38).

Protein Extraction and co-IP Assay from *Arabidopsis* Seedlings. Co-IP assays were performed as previously described (20). Protein samples were detected with 1:1,000 diluted anti-RFP (AB233; Evrogen) for BORR:RFP detection and 1:2,000 diluted anti-Histone H3 (ab1791; Abcam) for Histone H3 as primary antibodies and subsequently with 1:10,000 diluted anti-rabbit IgG, HRP-linked secondary antibody (cytiva).

RT-qPCR Analysis. RT-qPCR assays were performed as previously described (38). *PP2A3* (AT1G13320) was used as the reference gene. Primer pairs for qPCR are described in *SI Appendix*, Table S1. All experiments were performed in three biological replicates.

Bioinformatics. To detect homologs of BORIs and Survivin in eukaryotes, we optimized multiple-profile HMMs based on iterative reciprocal similarity searches using various tools from the HMMER package version 3.1b2 (52), similar to a strategy used in our previous work (19, 53). For eukaryotic sequence searches, we used a variety of large databases (53–55) (Datasets S5 and S6). For prokaryotic sequences, we performed online jackhmmer searches against UniProt (56). Maximum-likelihood phylogenetic analyses (Datasets S3 and S4) were performed with IQ-Tree (version 1.6.12) using model selection, including the assessment of all mixture models, 1000 UF bootstrap, and SH-like approximate likelihood ratio test replicates (57).

Data, Materials, and Software Availability. Sequence alignments, structures, predictions, and phylogenetic analyses have been deposited in Figshare (10.6084/m9.figshare.17840213) (61).

ACKNOWLEDGMENTS. We thank Mariana Motta (University of Hamburg) for critical reading and helpful comments on the manuscript. E.C.T. is supported by a personal fellowship from the Nederlandse Organisatie voor Wetenschappelijk Onderzoek (grant no. VI.Veni.202.223). This work was supported by the Deutsche Forschungsgemeinschaft (grant no. SCHN 736/8–1) to A.S., a grant from the Ohsumi Frontier Science Foundation to S.K., and the Japan Society for the Promotion of Science (KAKENHI grant no. JP21K06215) to S.K.

1. M. R. Motta, A. Schnittger, A microtubule perspective on plant cell division. *Curr. Biol.* **31**, R547–R552 (2021).
2. E. C. Tromer, J. J. E. van Hooff, G. J. P. L. Kops, B. Snel, Mosaic origin of the eukaryotic kinetochore. *Proc. Natl. Acad. Sci. U.S.A.* **116**, 12873–12882 (2019).
3. A. Musacchio, A. Desai, A molecular view of kinetochore assembly and function. *Biology (Basel)* **6**, 5 (2017).
4. S. Müller, G. Jürgens, Plant cytokinesis-No ring, no constriction but centrifugal construction of the partitioning membrane. *Semin. Cell Dev. Biol.* **53**, 10–18 (2016).
5. J. R. Brown, K. K. Koretke, M. L. Birkeland, P. Sanseau, D. R. Patrick, Evolutionary relationships of Aurora kinases: Implications for model organism studies and the development of anti-cancer drugs. *BMC Evol. Biol.* **4**, 39 (2004).
6. M. Carmena, M. Wheelock, H. Funabiki, W. C. Earnshaw, The chromosomal passenger complex (CPC): From easy rider to the godfather of mitosis. *Nat. Rev. Mol. Cell Biol.* **13**, 789–803 (2012).
7. A. van der Horst, S. M. A. Lens, Cell division: Control of the chromosomal passenger complex in time and space. *Chromosoma* **123**, 25–42 (2014).
8. M. A. Abad *et al.*, Borealin-nucleosome interaction secures chromosome association of the chromosomal passenger complex. *J. Cell Biol.* **218**, 3912–3925 (2019).
9. F. Wang *et al.*, A positive feedback loop involving Haspin and Aurora B promotes CPC accumulation at centromeres in mitosis. *Curr. Biol.* **21**, 1061–1069 (2011).
10. F. Wang *et al.*, Histone H3 Thr-3 phosphorylation by Haspin positions Aurora B at centromeres in mitosis. *Science* **330**, 231–235 (2010).
11. A. E. Kelly *et al.*, Survivin reads phosphorylated histone H3 threonine 3 to activate the mitotic kinase Aurora B. *Science* **330**, 235–239 (2010).
12. Y. Yamagishi, T. Honda, Y. Tanno, Y. Watanabe, Two histone marks establish the inner centromere and chromosome bi-orientation. *Science* **330**, 239–243 (2010).
13. M. A. Abad *et al.*, Molecular basis for CPC-Sgo1 interaction: Implications for centromere localisation and function of the CPC. *bioRxiv*, 2021.08.27.457910 (2021).
14. M. A. Hadders *et al.*, Untangling the contribution of Haspin and Bub1 to Aurora B function during mitosis. *J. Cell Biol.* **219**, e201907087 (2020).
15. A. J. Broad, K. F. DeLuca, J. G. DeLuca, Aurora B kinase is recruited to multiple discrete kinetochore and centromere regions in human cells. *J. Cell Biol.* **219**, e201905144 (2020).
16. C. Liang *et al.*, Centromere-localized Aurora B kinase is required for the fidelity of chromosome segregation. *J. Cell Biol.* **219**, e201907092 (2020).
17. M. A. Hadders, S. M. A. Lens, Changing places: Chromosomal Passenger Complex relocation in early anaphase. *Trends Cell Biol.* **32**, 165–176 (2022).
18. O. Kirioukhova *et al.*, Female gametophytic cell specification and seed development require the function of the putative Arabidopsis INCENP ortholog WYRD. *Development* **138**, 3409–3420 (2011).
19. J. J. van Hooff, E. Tromer, L. M. van Wijk, B. Snel, G. J. Kops, Evolutionary dynamics of the kinetochore network in eukaryotes as revealed by comparative genomics. *EMBO Rep.* **18**, 1559–1571 (2017).
20. S. Komaki *et al.*, Functional analysis of the plant Chromosomal Passenger Complex. *Plant Physiol.* **183**, 1586–1599 (2020).
21. D. Kurihara, S. Matsunaga, T. Omura, T. Higashiyama, K. Fukui, Identification and characterization of plant Haspin kinase as a histone H3 threonine kinase. *BMC Plant Biol.* **11**, 73 (2011).
22. E. Kozgunova, T. Suzuki, M. Ito, T. Higashiyama, D. Kurihara, Haspin has multiple functions in the plant cell division regulatory network. *Plant Cell Physiol.* **57**, 848–861 (2016).
23. Y. Liu, C. Wang, H. Su, J. A. Birchler, F. Han, Phosphorylation of histone H3 by Haspin regulates chromosome alignment and segregation during mitosis in maize. *J. Exp. Bot.* **72**, 1046–1058 (2021).
24. Q. L. Deveraux, J. C. Reed, IAP family proteins–Suppressors of apoptosis. *Genes Dev.* **13**, 239–252 (1999).
25. S. P. Wheatley, D. C. Altieri, Survivin at a glance. *J. Cell Sci.* **132**, jcs223826 (2019).
26. K. Higashi *et al.*, Identification of a novel gene family, paralogs of inhibitor of apoptosis proteins present in plants, fungi, and animals. *Apoptosis* **10**, 471–480 (2005).
27. A. Daneva, Z. Gao, M. Van Durme, M. K. Nowack, Functions and regulation of programmed cell death in plant development. *Annu. Rev. Cell Dev. Biol.* **32**, 441–468 (2016).
28. E. A. Minina *et al.*, Apoptosis is not conserved in plants as revealed by critical examination of a model for plant apoptosis-like cell death. *BMC Biol.* **19**, 100 (2021).
29. J. Van Leene *et al.*, An improved toolbox to unravel the plant cellular machinery by tandem affinity purification of Arabidopsis protein complexes. *Nat. Protoc.* **10**, 169–187 (2015).
30. M. Desai, R. Pan, J. Hu, Arabidopsis Forkhead-Associated Domain Protein 3 negatively regulates peroxisome division. *J. Integr. Plant Biol.* **59**, 454–458 (2017).
31. D. Durocher, S. P. Jackson, The FHA domain. *FEBS Lett.* **513**, 58–66 (2002).
32. N. Coquelle, J. N. M. Glover, FHA domain pThr binding specificity: It's all about me. *Structure* **18**, 1549–1550 (2010).
33. A. W. Almawi, L. A. Matthews, A. Guarné, FHA domains: Phosphopeptide binding and beyond. *Prog. Biophys. Mol. Biol.* **127**, 105–110 (2017).
34. J. R. Allen, E. G. Wilkinson, L. C. Strader, Creativity comes from interactions: Modules of protein interactions in plants. *FEBS J.* **289**, 1492–1514 (2022).
35. J. M. Stone, M. A. Collinge, R. D. Smith, M. A. Horn, J. C. Walker, Interaction of a protein phosphatase with an Arabidopsis serine-threonine receptor kinase. *Science* **266**, 793–795 (1994).
36. R. W. Williams, J. M. Wilson, E. M. Meyerowitz, A possible role for kinase-associated protein phosphatase in the Arabidopsis CLAVATA1 signaling pathway. *Proc. Natl. Acad. Sci. U.S.A.* **94**, 10467–10472 (1997).
37. I. M. Rienties, J. Vink, J. W. Borst, E. Russinova, S. C. de Vries, The Arabidopsis SERK1 protein interacts with the AAA-ATPase AtCDC48, the 14-3-3 protein GF14lambda and the PP2C phosphatase KAPP. *Planta* **221**, 394–405 (2005).
38. S. Komaki, A. Schnittger, The spindle assembly checkpoint in Arabidopsis is rapidly shut off during severe stress. *Dev. Cell* **43**, 172–185.e5 (2017).
39. I. J. Byeon, S. Yongkiettrakul, M. D. Tsai, Solution structure of the yeast Rad53 FHA2 complexed with a phosphothreonine peptide pTXXL: Comparison with the structures of FHA2-pYXL and FHA1-pTXXD complexes. *J. Mol. Biol.* **314**, 577–588 (2001).
40. L. J. Alderwick *et al.*, Molecular structure of EmbR, a response element of Ser/Thr kinase signaling in Mycobacterium tuberculosis. *Proc. Natl. Acad. Sci. U.S.A.* **103**, 2558–2563 (2006).
41. J. Liu *et al.*, Structural mechanism of the phosphorylation-dependent dimerization of the MDC1 forkhead-associated domain. *Nucleic Acids Res.* **40**, 3898–3912 (2012).
42. G.-I. Lee, Z. Ding, J. C. Walker, S. R. Van Doren, NMR structure of the forkhead-associated domain from the Arabidopsis receptor kinase-associated protein phosphatase. *Proc. Natl. Acad. Sci. U.S.A.* **100**, 11261–11266 (2003).
43. J. Eswaran *et al.*, Structure and functional characterization of the atypical human kinase haspin. *Proc. Natl. Acad. Sci. U.S.A.* **106**, 20198–20203 (2009).
44. M. Serena, R. N. Bastos, P. R. Elliott, F. A. Barr, Molecular basis of MKLP2-dependent Aurora B transport from chromatin to the anaphase central spindle. *J. Cell Biol.* **219**, e201910059 (2020).
45. I. E. Adriaans *et al.*, MKLP2 is a motile kinesin that transports the chromosomal passenger complex during anaphase. *Curr. Biol.* **30**, 2628–2637.e9 (2020).
46. Y. Hoshino, E. A. Gaucher, Evolution of bacterial steroid biosynthesis and its impact on eukaryogenesis. *Proc. Natl. Acad. Sci. U.S.A.* **118**, e2101276118 (2021).
47. P. López-García, D. Moreira, The Syntrophy hypothesis for the origin of eukaryotes revisited. *Nat. Microbiol.* **5**, 655–667 (2020).
48. S. Henikoff, K. Ahmad, H. S. Malik, The centromere paradox: Stable inheritance with rapidly evolving DNA. *Science* **293**, 1098–1102 (2001).
49. T. Kumon *et al.*, Parallel pathways for recruiting effector proteins determine centromere drive and suppression. *Cell* **184**, 4904–4918.e11 (2021).
50. T. Akera, E. Trimm, M. A. Lampson, Molecular strategies of meiotic cheating by selfish centromeres. *Cell* **178**, 1132–1144.e10 (2019).
51. J. Van Leene *et al.*, Isolation of transcription factor complexes from Arabidopsis cell suspension cultures by tandem affinity purification. *Methods Mol. Biol.* **754**, 195–218 (2011).
52. S. R. Eddy, Accelerated Profile HMM Searches. *PLOS Comput. Biol.* **7**, e1002195 (2011).
53. E. C. Tromer, T. A. Wemyss, P. Ludzia, R. F. Waller, B. Akiyoshi, Repurposing of synaptonemal complex proteins for kinetochores in Kinetoplastida. *Open Biol.* **11**, 210049 (2021).

54. D. J. Richter, C. Berney, J. F. H. Strassert, F. Burki, C. de Vargas, EukProt: A database of genome-scale predicted proteins across the diversity of eukaryotic life. 2020.06.30.180687 (2020).
55. UniProt Consortium, UniProt: A worldwide hub of protein knowledge. *Nucleic Acids Res.* **47** (D1), D506–D515 (2019).
56. R. D. Finn *et al.*, HMMER web server: 2015 update. *Nucleic Acids Res.* **43** (W1), W30–W38 (2015).
57. J. Trifinopoulos, L.-T. Nguyen, A. von Haeseler, B. Q. Minh, W-IQ-TREE: A fast online phylogenetic tool for maximum likelihood analysis. *Nucleic Acids Res.* **44** (W1), W232–W235 (2016).
58. J. Chen *et al.*, Histone H3 N-terminal mimicry drives a novel network of methyl-effector interactions. *Biochem. J.* **478**, 1943–1958 (2021).
59. W. F. Brandt, W. N. Strickland, M. Morgan, C. Von Holt, Comparison of the n-terminal amino acid sequences of histone F3 from a mammal, a bird, a shark, an echinoderm, a mollusc and a plant. *FEBS Lett.* **40**, 167–172 (1974).
60. F. Burki, A. J. Roger, M. W. Brown, A. G. B. Simpson, The new tree of eukaryotes. *Trends Ecol. Evol.* **35**, 43–55 (2020).
61. S. Komaki *et al.*, Molecular convergence by differential domain acquisition is a hallmark of chromosomal passenger complex evolution. Figshare. http://doi.org/10.6084/m9.figshare.17840213. Deposited 29 September 2022.